

Numerical simulation of tandem solar cells based-CIGS and C-Si sub-cells using SCAPS -1D

Amina Bouzidi ^{1,*}, Idris Bouchama ¹, Moufidi Hadjab ¹, M. A. Saeed ²

¹ Department of Electronics, Faculty of Technology, University Mohamed Boudiaf, 28000, M'sila, Algeria

² Department of Physics, Division of Science & Technology, University of Education, Lahore, Pakistan

*amina.bouzidi@univ-msila.dz

Abstract

Numerical simulation of single junction and tandem solar cells-based copper indium gallium diselenide Cu(In,Ga)Se₂ and silicon (c-Si) electrical characteristics have been accomplished by Solar Cell Capacitance Simulator (SCAPS 1-D) tool. The layered structure consisting of CIGS as top cell with a buffer layer of zinc-based oxysulfide Zn(O,S) and the bottom cell of c-Si junction has been investigated. The top and bottom single cells have demonstrated the conversion efficiency as 11.63 and 13.16%, respectively. The tandem designs exhibited a conversion efficiency of 25.68% resulted from the enhanced open-circuit voltage (V_{OC}) as 0.90 V and short-circuit current density (J_{SC}) as 36.99 mA/cm². The cells were illuminated via AM 1.5 to investigate the current densities and external quantum efficiency (EQE). The simulations were optimized by adjusting the CIGS concentration and the thickness of semiconducting layers. Moreover, the effect of variation in temperature on the device performance has been investigated.

Keywords: Tandem, SCAPS-1D, Buffer layer, Cu(In,Ga)Se₂ material, c-Si.

1. Introduction

The development of high-performance solar cells offers the viability of promising and large-scale terrestrial photovoltaic applications with high power per unit cost. GaAs, Si, CIGSe, CdTe, and perovskite based single-junction solar cells developed with reasonable efficiency [1]. However, single-junction solar cells can attain AM1.5 efficiency up to 30–32% [2]. The state-of-the-art of single junction solar cells are approaching the Shockley–Queisser limit and the developments in solar cells in context of their efficiency need to consider multi-junctions (MJ) with a variety of band gaps that are capable to cater large solar spectrum [3–5]. The MJ approach would help to reduce thermalization and below-band-gap losses due to the utilization of photons having wide range of frequencies [6]. The photon with higher energies would be absorbed by small band gap materials and resulted in thermalization loss however; photons with smaller energies would be

used to excite electrons in high band gap materials and resulted in below-band-gap loss.

In the near future, Si-based tandem solar cells [7] such as III–V/Si [8,9], II–VI/Si [10], chalcopyrite/Si [11], CZTS/Si [12], and perovskite/Si [13] are expected to play a vital role. Furthermore, MJ solar cells approach like perovskite/perovskite [14], III–V/CIGSe [15], and perovskite/CIGSe [16] has strong potential to make MJ solar cells as promising and potential candidates for optoelectronic applications especially, photovoltaic energy conversion [17].

The Si (bottom cell) based tandem solar cells are essential, because they are the direct way to go beyond the single-junction efficiency limit [18]. In addition, solar cells involving crystalline silicon are the dominant technology on the commercial market of photovoltaic with 66% of total demand in 2020 [19]. The CIGS as top cell absorber becomes an exciting candidate since it offers high efficiency, long-term stability in addition to the low-cost production [20]. CIGS is a very suitable

material with high optical absorption coefficient in the visible region, which is excellent as compared to silicon [20, 21]. Moreover, the CIGS solar cells exhibit tunable band-gap with exceptional outdoor stability and radiation hardness. The CIGS solar cells offer power up to 919 W/Kg, which is high amongst all kinds of solar cells. Most recently, the Centre of Solar Energy and Hydrogen Research (ZSW) [21] and National Renewable Energy Laboratory (NREL) [22] reported the efficiency of CIGS thin film solar cell with an active area of 0.5 cm² as 20.3 and 19.9%, respectively. It has also been reported that CIGS thin films have demonstrated the tunable band-gap energy from 1.04 to 1.68 eV with varying Ga content from $x = 0$ to 1 [23]. A theoretical study of tandem cell CIGS/CIS has been reported by Kim *et al.* with an efficiency of 26.7% [24]. Nacer *et al.* reported the optimized investigations on current matching double junction InGaN /Si solar cells with an efficiency of 38.3% [25]. Novel designs of CZTS/Si and chalcopyrite/Si tandem cells have recently been reported with efficiencies as 22.9 and 19.8%, respectively by L. Aimin [26] and Kim *et al.* [11].

In the current work, potential efficiencies of CIGS/Si tandem cells are addressed using the SCAPS-1D simulation tool. Firstly, simulations for external quantum efficiency (EQE) and J(V) characteristics has been carried out in independent conditions as well as with the effect of different thicknesses for absorber and buffer layers in CIGS and Si based single-junction cells. Secondly, in accordance with the obtained results, the investigations were expanded for CIGS solar cell structure in order to simulate the J(V) characteristics as a function of concentration x . Furthermore, for tandem structure of cell, CIGS/Si tandem solar cell was simulated and improvements in the solar cell performance have been observed in comparison to the CIGS and Si single-junction solar cells. Finally, the influence of working temperature on the efficiency and other parameters of tandem solar cell has also been studied.

2. Structure and parameters of solar cell

The designed structure of CIGS/c-Si tandem cell is shown in Fig. 1. CIGS having large band-gap of

1.69 eV was used as top cell and c-Si with low band-gap of 1.16 eV was used bottom cell. The thickness of top cell was kept smaller as compared to that for bottom cell [21]. The photovoltaic device with top and bottom complementary absorbing sub-cells of different band gap was used to absorb the incident photons of higher energy. Mostly, the selection criteria for these cells would be as; the bottom cell may generate high currents with low open circuit voltage as compared to the top cell [27].

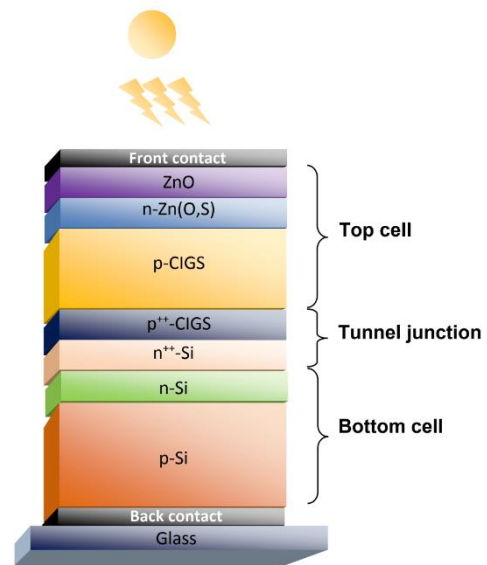


Fig.1. Schematic of proposed two-terminal CIGS/Si tandem solar cell with tunnel junction.

The tandem chalcopyrite-on-silicon cell composed of top ZnO/n-Zn(O,S)/p-CIGS and bottom n-Si/p-Si hetero-junction utilizing monolithically integrated two terminals (2-T).

In a tandem cell with two terminals, there must be an ohmic contact between two consecutive cells. Internal ohmic contacts (IOCs) exhibit some novel properties like higher conductivities and optical transparency, although, high pick current density is one of the most significant property of IOCs. The IOCs can be prepared by two methods, one method is tunnel junctions (or tunnel diode or recombination layers) and the other one is metal interconnects. However, the later method may be avoided owing to its complex processing and poor device efficiency [28]. As mentioned earlier that c-Si cell (bottom cell) and CIGS (top cell) are connected by a tunnel junction delimited by two

regions P and N, with high doping concentrations [P^{++} - CIGS / n^{++} - Si].

The investigations on the performance of this tandem solar cell have been carried out through Solar Cell Capacitance Simulator (SCAPS-1D, version 3.3.06) tool under AM1.5 illumination. SCAPS-1D was developed at the Department of Electronics and Information Systems, University of Gent, Belgium and offers seven input semiconductor layers to be studied via one-dimensional simulation [29]. Moreover, this tool is capable to measure the light bias, lighting from either the n-side or p-side, quantum and power conversion efficiency, frequency response, band structure, fill factor, open-circuit voltage and capacitance-voltage characteristics, short-current density, temperature profile, generation and recombination profile, electric field distribution and spectral performance [30]. In the current study, the operating temperature of solar cells was set to be 300 K. The input parameters used for simulation are given in **Table.1**.

Table 1. Input parameters used for the SCAPS-1D simulations

CIGS solar cell Parameters and unit	p-CIGS	n-Zn(O,S)		ZnO
		n-ZnO	n-ZnS	
Thickness (μm)	2	0.03	0.03	0.01
Band-Gap (eV)	1.69	3.3	2.26	3.3
Electron Affinity, E_a (eV)	4.8	4.45	3.5	4.45
Relative dielectric permittivity (ϵ_r)	13.6	9	9.67	9
Hole mobility, μ_p ($\text{cm}^2 \text{V}^{-1} \text{s}^{-1}$)	25	25	80	25
Electron mobility, μ_n ($\text{cm}^2 \text{V}^{-1} \text{s}^{-1}$)	100	100	330	100
Donor density, N_D (cm^{-3})	-	2×10^{18}	2×10^{18}	1×10^{10}
Acceptor density, N_A (cm^{-3})	1×10^{15}	-	-	-
References	[53]	[51]	[51]	[51]

Silicon solar cell Parameters and unit	p - Si	n - Si
Thickness (μm)	450	1
Band-Gap (eV)	1.12	1.12
Electron Affinity, E_a (eV)	4.05	4.05
Relative dielectric permittivity (ϵ_r)	11.9	11.9
Hole mobility, μ_p ($\text{cm}^2 \text{V}^{-1} \text{s}^{-1}$)	450	450
Electron mobility, μ_n ($\text{cm}^2 \text{V}^{-1} \text{s}^{-1}$)	1500	1500
Donor density, N_D (cm^{-3})	-	1×10^{16}
Acceptor density, N_A (cm^{-3})	1×10^{15}	-
References	[54]	[54]

3. Results and discussion

Optimization of photovoltaic parameters for a tandem CIGS/c-Si solar cell has been performed in context to improve the stability and efficiency of already available commercial devices. The optimization of designed cells was done through variations in thickness and concentration x of the respective layers. Firstly, CIGS and Si single junction cell was designed and optimized followed by the study of two single junction cells incorporated with n^{++} -Si / p^{++} -CIGS tunnel junction. Finally, the proposed tandem cell was optimized with respect to layer thickness and band-gap.

3.1. Simulations of single cell junction

3.1.1. Variation in J(V) and EQE curves

The effect of variation in thickness of absorber and buffer layers for both *i.e.*, top and bottom cells have been investigated and J(V) characteristics and the external quantum efficiency (EQE) curves for top and bottom cells are shown in **Fig. 2** and **3**, respectively. The EQE for a photovoltaic cell is the ratio of short-circuit current $J_{SC}(\lambda)$ and the incident photon flux $\phi_0(\lambda)$ at a particular energy multiplied by the charge q of electrons [33]:

$$EQE(\lambda) = \frac{J_{sc}(\lambda)}{q \phi_0(\lambda)} \quad (1)$$

Fig. 2.a and 3.a illustrate that for both the cells, current densities J(V) observed to decrease as a function of absorption layer thickness. However, current densities for the buffer layer observed to increase with the increment in thickness as shown in Fig. 2.b and 3.b. The effect of increment in absorption layer thickness resulted in higher EQE for both cells as shown in Fig. 2.c and 3.c. This increment in EQE is observed to be significant at higher wavelength.

However, when the thickness of buffer layer enhanced, there is a relative decrease in EQE as represented in Fig. 2.d and 3.d.

The significant increment in J(V) and EQE observed to saturate at the higher values of thickness for longer wavelengths since the incident photons with low wavelengths are absorbed near the surface [34].

3.1.2. Effects of layer thickness on top cell

The absorber layer thickness of p-CIGS was varied from 0.2 to 4.5 μm and the effect of thickness increase on the efficiency is depicted in Fig. 4.a. This significant increase in efficiency resulted from the creation of maximum electron-hole pairs due to photon absorption in the layer with large thickness. Moreover, it has been observed that fill factor, J_{SC} and V_{OC} also increase with increasing thickness of absorber layer.

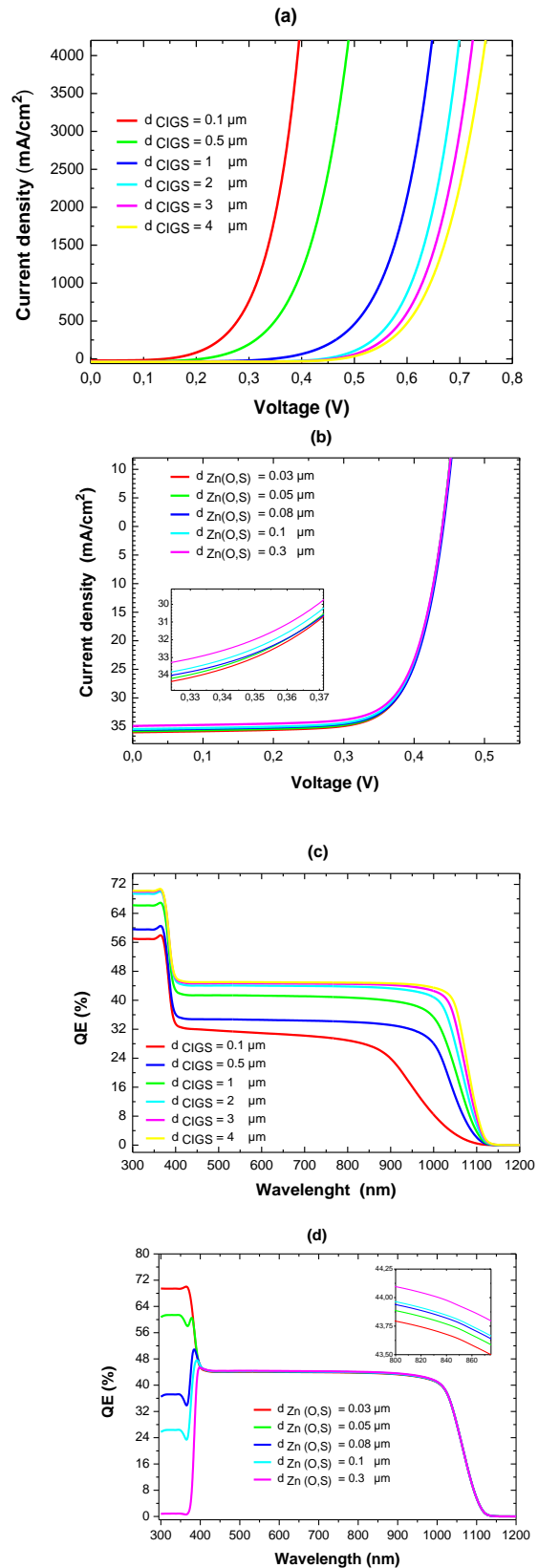


Fig.2. Variation of J(V) and EQE curves to the varying thickness of the top cell: (a) variation J-V of the absorber p-CIGS, (b) variation J-V of the buffer layer n-Zn (O, S), (c) variation EQE of the absorber p-CIGS and (d) variation EQE of the buffer layer n-Zn (O, S).

Fig. 4.b shows the decrease in fill factor as the thickness of buffer layer n-Zn (O, S) varied from 0.01 to 0.3 μm . The V_{OC} observed to remain constant as the buffer layer thickness increases, although, the efficiency and J_{SC} with the highest value (11.63%, 36.01 mA /cm² respectively) at 0.03 μm thickness starts decreasing for further increase in thickness of the buffer layer.

3.1.3. Effect of layer thickness on bottom cell

The thickness of absorber layer p-Si was varied from 50 to 500 μm and improvement in efficiency and J_{SC} has been observed as function of thickness while the Fill factor and V_{OC} remains unchanged as shown in **Fig. 5.a**. The thickness of absorber layer n-Si was varied from 0.1 to 3 μm and decrement in efficiency and J_{SC} has been observed as a function of layer thickness while, fill factor and V_{OC} are observed to increase. It is important to mention here that, an absorber layer with suitable thickness is required to capture maximum number of incident photons with a direct consequence as a significant increase in the efficiency while reducing the fill factor.

3.1.4. Effect thickness of CIGS with different composition x

The ultimate aim of the study was to attain an optimum fraction x in composition of the $\text{CuIn}_{1-x}\text{Ga}_x\text{Se}_2$ cell in addition to the optimized band gap and affinity to advance the overall cell performance. In a CIGS solar cell, fraction x determines the density of Gallium in the structure that can be defined as per following equation [35, 36]:

$$x = \frac{G_a}{G_a + I_n} \quad (2)$$

Earlier published experimental data for CIGS solar cells revealed that variation in affinity and band gap versus fraction x can be formulated as per following equations [37]:

$$E_g = 1.04 + 0.391x + 0.262 x^2 \quad (3)$$

$$\chi = 4.61 + 1.162x + 0.034 x^2 \quad (4)$$

Fig. 6 shows that in accordance with the semiconductor physics theory, the affinity of the

cell structure decreases as the band gap increases with variation in fraction x [38].

In a solar cell, the two important figures of merits are fill factor (FF) and efficiency (η) of the device.

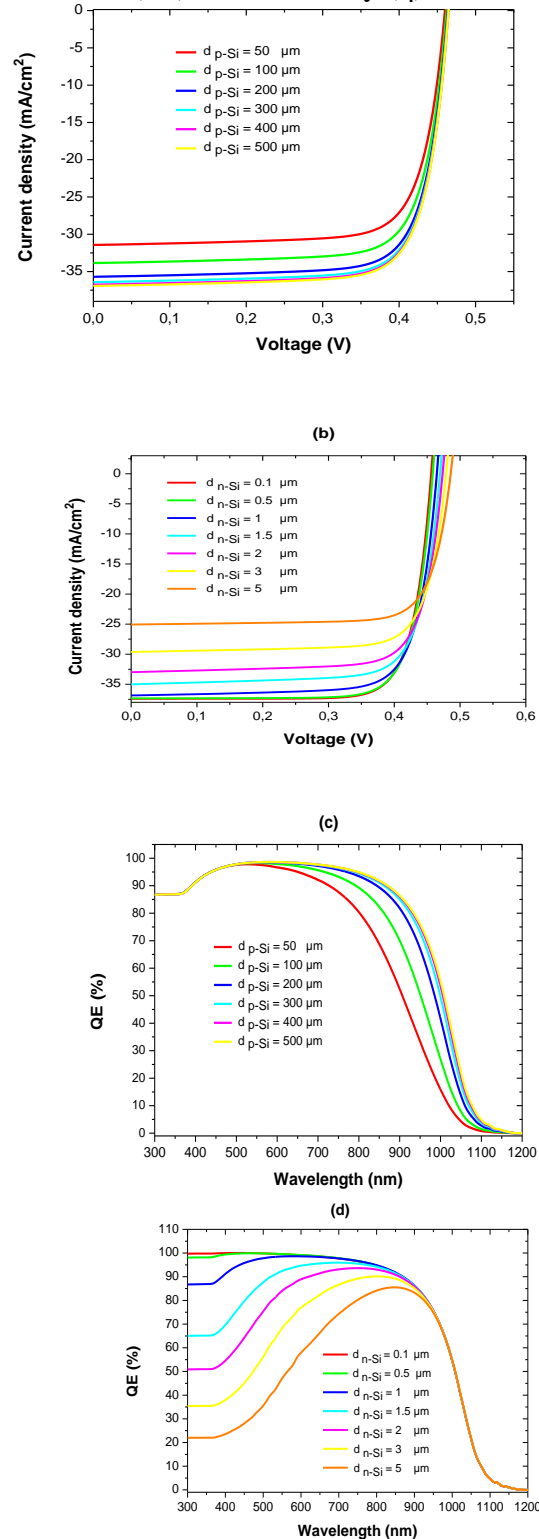


Fig.3. Variation of J(V) and EQE curves to the varying thickness of the bottom cell: (a) variation J-V of the absorber p-Si, (b) variation J-V of the buffer layer n-Si, (c) variation EQE of the absorber p-Si and (d) variation EQE of the buffer layer n-Si.

The η demonstrated the power conversion efficiency of the device while FF represented the measure of queerness in J(V) characteristics of the device and usually, it has a value less than one. The equations below express these factors as;

$$FF = \frac{V_{mP} I_{mP}}{V_{OC} J_{SC}} \quad (5)$$

$$\eta = \frac{FF V_{OC} J_{SC}}{P_{in}} \quad (6)$$

Where I_{mP} and V_{mP} represent the current and voltage to attain the maximum power of device and P_{in} represents the power of incident photons as decided by the input wavelength spectrum.

Fig. 7 depicts the illuminated J(V) characteristics of top cell CIGS with various concentration of x i.e., 0.24, 0.33, 0.49, and 0.6 eV with respect to the thickness of absorber layer. Firstly, V_{OC} observed to increase as a function of increasing thickness and at $x \geq 0.49$, the V_{OC} increases until the thickness of absorber layer is $0.7 \mu\text{m}$ and decreases afterwards as depicted in **Fig. 7.a** in consequence of the direct relation between V_{OC} and band gap as $V_{OC} = 1/q \times E_g$, where q represents the elemental charge [39]. Additionally, the simulations revealed that J_{SC} increases as a function of absorber layer thickness however, the growth as a function of fraction x is slightly slow as shown in **Fig. 7.b**. The fill factor observed to increase with increasing thickness of absorber layer and decreases for $x \leq 0.6$ as shown in **Fig. 7.c**. **Fig. 7.d** shows the efficiencies of the CIGS solar cell increases up to thickness of $1 \mu\text{m}$, beyond this point the efficiencies clearly begin to decrease with increasing fraction x .

3.2. Chalcopyrite/Silicon tandem solar cell

The structural design of proposed dual junction CIGS/c-Si solar cell is given in **Fig. 1**. **Fig. 8** shows the J(V) characteristics in CIGS (top cell), c-Si (bottom cell) and CIGS/Si (tandem cell). The experimental results of the conversion efficiencies of the considered solar cells fabricated by various deposition techniques are given in **Table 2**. From literature [40-43], we confirm that the revealed results of p-CIGS /n-Zn(O,S) and p-Si/n-Si based solar cell works successfully at improved efficiency.

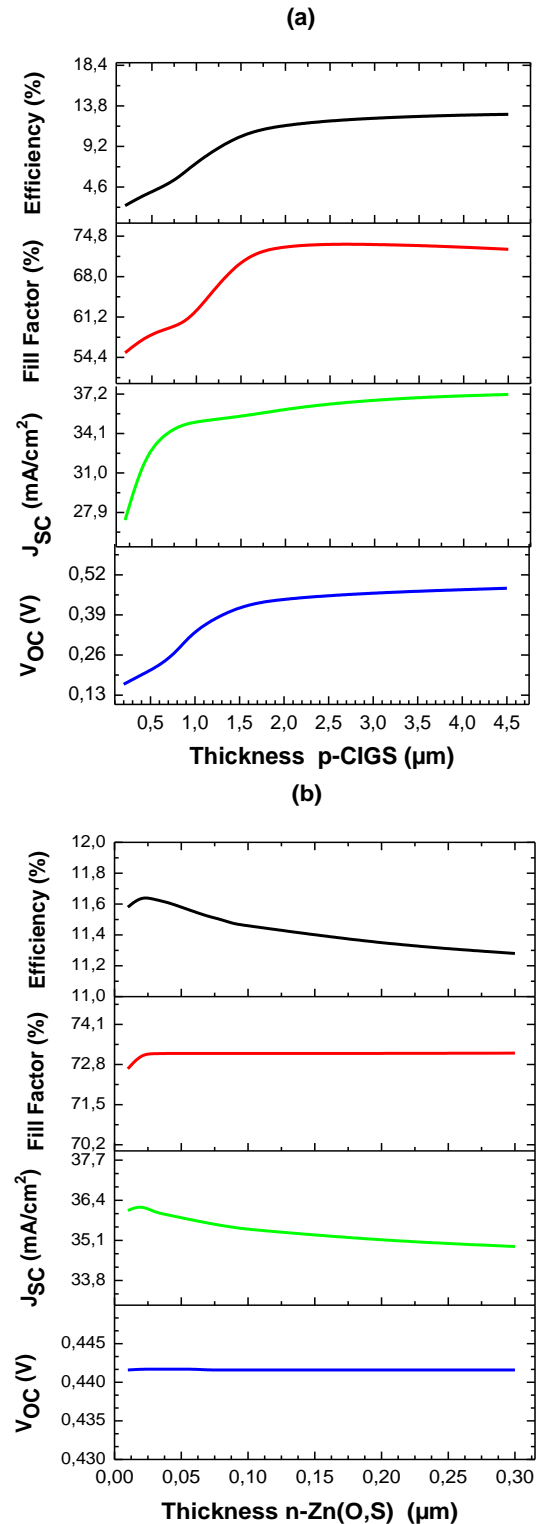


Fig.4. J(V) curve of top cell variation with the thickness of: (a) absorber layer and (b) buffer layer.

Table 2. The experimental results of efficiencies of CIGS and Si solar cells.

Absorber/ Buffer layer	Method	Efficiency (%)	Ref.
p-CIGS /n- Zn(O,S)	Chemical bath deposition	6.4	[40]
	Co-Sputtering	9.05	[41]
	Sputtering	13.0	[42]
p-Si/n-Si	thermal and chemical	13.0	[43]

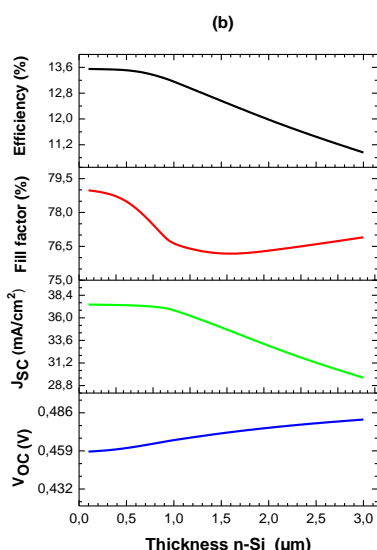
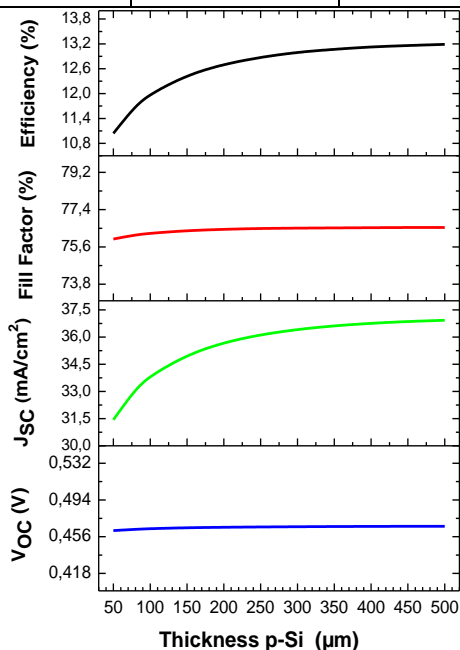


Fig.5. J(V) curve of bottom cell variation with the thickness of: (a) absorber and (b) buffer layer.

Two-terminal tandem solar cell electrically operated exactly in a same manner as two diodes operate when connected in series. The short circuit current density of tandem cell *i.e.*, 36.99 mA/cm^2 is close to that for bottom cell (Si) and top cell (CIGS) *i.e.*, 36.85 mA/cm^2 and 36.01 mA/cm^2 , respectively. The open circuit voltage of tandem design *i.e.*, 0.90 V is exactly equal to the sum of open circuit voltage for Si and CIGS cells *i.e.*, 0.46 V and 0.44 V , respectively. From these observations, one can conclude that operation of the tandem cell is likewise the operation of Si and CIGS cells connected in series. However, the FF for the tandem cell *i.e.*, 76.93% is slightly higher than that for Si and CIGS single junction cells *i.e.*, 76.54 and 73.15% , respectively. Enhanced V_{OC} and FF resulted in improved conversion efficiency in case of tandem cells *i.e.*, 25.68% , that is significantly higher than the conversion efficiencies of Si and CIGS single junction solar cells *i.e.*, 13.16 and 11.63% , respectively).

Table. 3 summarize the simulated results of different parameters of Silicon (Si), chalcopyrite (CIGS) and CIGS /Si tandem solar cells.

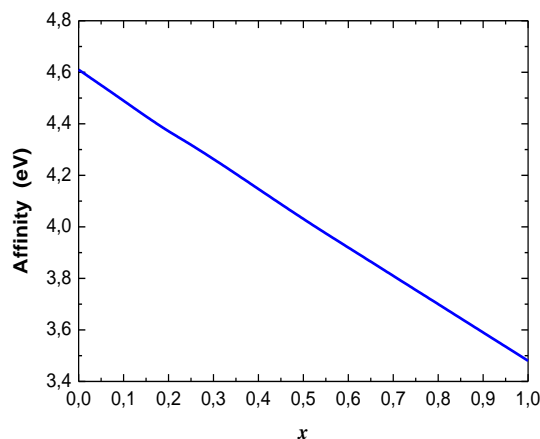


Fig.6. Affinity percentage, versus x composition fraction for the solar cell.

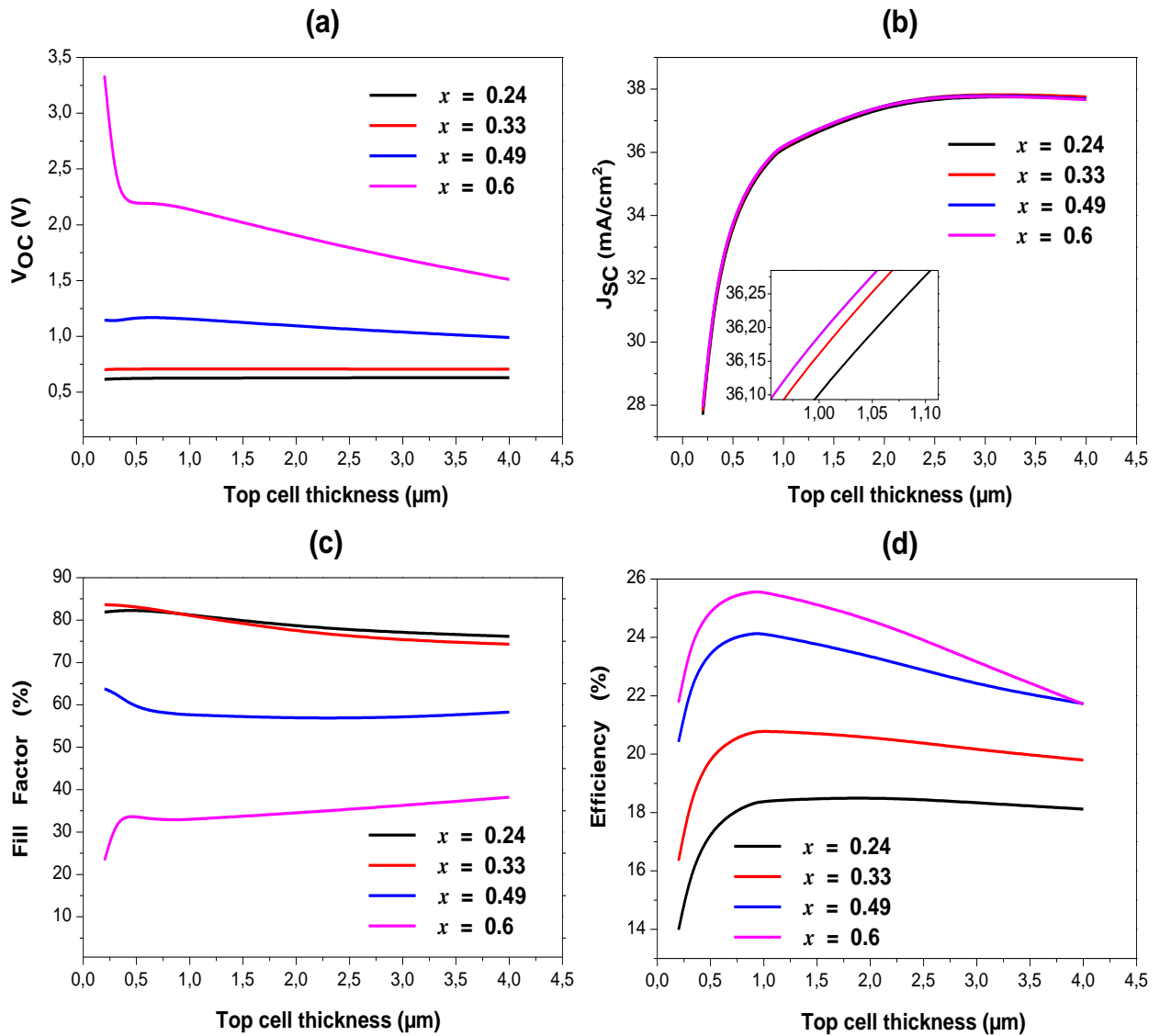


Fig.7. Simulated J-V characteristics of CIGS ($x = 0.24, 0.33, 0.49,$ and 0.6) with respect to their absorber thickness: (a) V_{OC} , (b) J_{SC} , (c) fill factor, and (d) Efficiency.

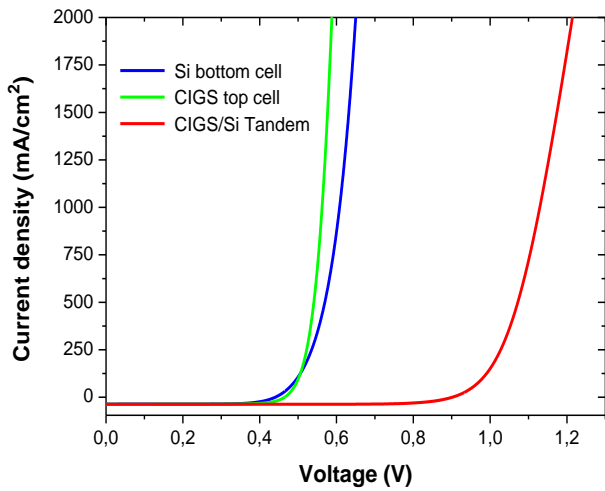


Fig. 8. J(V) characteristics for the CIGS top cell, Si bottom cell and CIGS/Si tandem cell.

3.2.1. Temperature dependence of CIGS/Si tandem cell parameters

Since the overall cell operation can be effected by the temperature, the effect of temperature on various parameters of the proposed tandem cell is shown in Fig. 9. The effect of temperature on the parameters like V_{OC} , J_{SC} , η and FF has been investigated.

The significant reduction in V_{OC} as a function of temperature is due to enhanced reverse saturation current density as there is an exponential dependence of intrinsic carrier concentration on temperature as shown by the relation [25]:

$$n_{i1,2}^2 = N_{c1,2} N_{v1,2} \exp\left(-\frac{E_{g1,2}}{kT}\right) \quad (7)$$

where k is the Boltzmann constant, N_c and N_v are the effective densities of states for the sub-cells given as:

$$N_{c,v} (cm^{-3}) = 2,5 \cdot 10^{19} \left(\frac{m_{n,p}^*}{m_0}\right)^{1.5} \left(\frac{T}{300}\right)^{1.5} \quad (8)$$

$m_{n,p}^*$ are the carrier effective masses.

The band gap is inversely related to the temperature as; [34]:

$$E_g(T) = E_g(0) - \frac{\alpha T^2}{T + \beta} \quad (9)$$

where $E_g(T)$ is the band gap of the material at a particular temperature T , and α and β are the constants.

Fig. 10 shows the J(V) curve for tandem solar cell at temperature range from 300 to 500 K. In conclusion, one can judiciously speculate that with

increasing temperature of the device, the efficiency of the cell may be compromised.

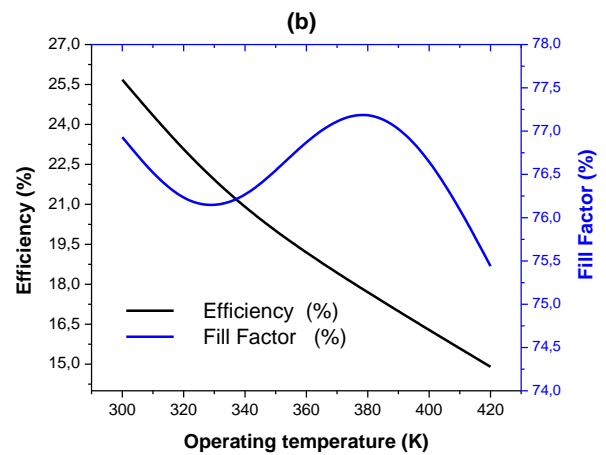
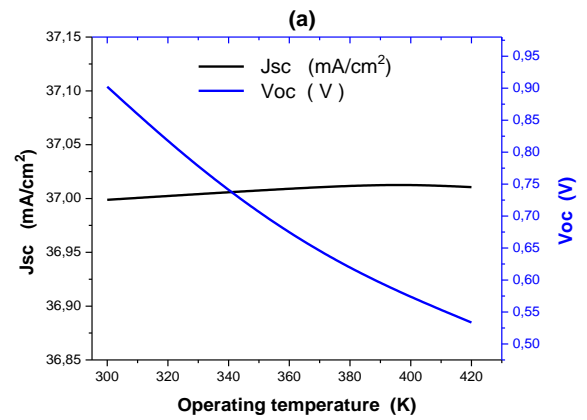


Fig. 9. Variations of the short-circuit current (J_{SC}) and the open circuit voltage (V_{OC}) (a) the fill factor (FF) and the conversion efficiency (η) (b) as a function of the temperature.

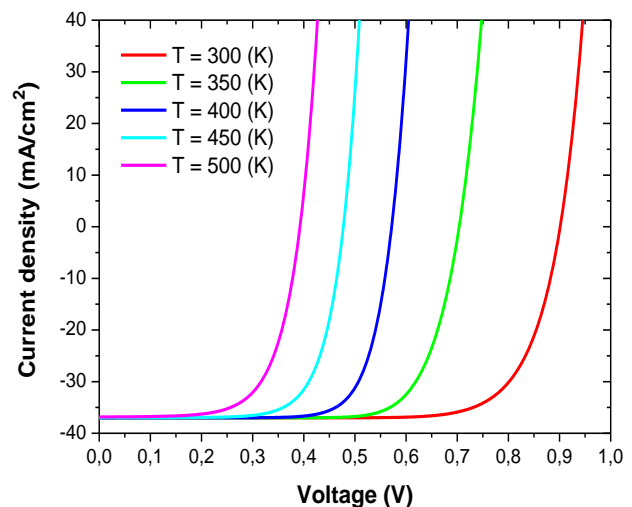


Fig.10. Effect of the working temperature on the J(V) curve of the tandem solar cell.

Our results for the three proposed structures of CIGS, c-Si and CIGS/Si tandem cell based solar cells are given in **Table 3** and the optimized efficiency compared with published data [12, 24-27, 32, 34, 44-48] for double junction solar cell is summarized in **Table 4**.

Table 3. Summary of performance results of Si, CIGS single cell and CIGS /Si tandem solar cell.

Parameters	V _{oc} (V)	J _{sc} (mA/cm ²)	FF (%)	η(%)
Si Bottom Cell	0.46	36.85	76.54	13.16
CIGS Top Cell	0.44	36.01	73.15	11.63
CIGS /Si Tandem Cell	0.90	36.99	76.93	25.68

Table 4. Comparison between the proposed structures with other works.

Structure	Conversion efficiency (%)	References
CIGS/Si	25.68	This work
	26.7	[12]
CIGS/CIS	19.8	[24]
InGaN/Si	38.3	[25]
CZTS/Si	22.9	[26]
Cu ₂ O/Si	31.23	[27]
GaInP/Si	31.11	[32]
CdTe/Si	28.45	[44]
	26.71	[45]
Perovskite/Si	28.71	[46]
	24.4	[34]
	33.67	[48]
Perovskite/perovskite	24.86	[47]

4. Conclusion

In summary, a theoretical framework on two terminals CIGS/Si tandem cell with [p⁺⁺- CIGS/n⁺⁺-Si] tunnel junction was designed followed by optimized simulations with the SCAPS 1-D tool to suggest optimum parameters for CIGS/Si based

solar cell. Simulations revealed that the proposed solar cell could offer 25.68% efficiency with V_{oc} of 0.90 V, J_{sc} of 36.99 mA/cm² and fill factor of 76.93%. The total thickness of the proposed tandem cell was of the order of 453 μm. The optimum thickness for the chalcopyrite and Si absorber layer is 2 and 450 μm, respectively and the optimized band gap for CIGS and Si material are 1.69 and 1.12 eV, respectively. The numerical simulation revealed that temperature of the device might be selected carefully since it has great impact on the overall performance of the solar cell. This work gives theoretical guidance towards the efficient realization of chalcopyrite/silicon based tandem solar cells by optimizing different cell parameters.

Future scope

In this work, the proposed tandem cell design may provide a pathway in the field of renewable energy since increasing demand of energy require potential research focus.

References

1. M. A. Green et al., Prog. Photovoltaics, 29 (3) (2021).
2. M. Yamaguchi, Phys. Status Solidi C 12, 489 (2015).
3. W. Shockley and H. J. Queisser, J. Appl. Phys., 32, 510 (1961).
4. M. Yamaguchi et al., Sol. Energy, 79 (78) (2005).
5. M. Yamaguchi, Clean Electricity from Photovoltaics, 2nd ed., edited by M. D. Archer and M. A. Green (Imperial College Press) 307 (2015).
6. L. C. Hirst and N. J. Ekins-Daukes, Prog. Photovoltaics, 19, 286 (2011).
7. M. Yamaguchi et al., J. Phys. D: Appl. Phys, 51, 133002 (2018).
8. S. Essig, et al., Nat. Energy, 2, 17144 (2017).
9. D. Lackner et al., Sol. RRL, 4, 2000210 (2020).
10. M. Carmody et al., Appl. Phys, 96, 153502 (2010).
11. K. Kim et al., Sol. Energy, 145, 52 (2017).
12. M. Valentini, et al., Sol. Energy, 190, 414 (2019).
13. S. Albrecht et al., paper presented at the 36th European Photovoltaic Solar Energy Conference, Marseille, France (2019).
14. R. Lin et al., Nat. Energy, 4, 864 (2019).
15. K. Makita et al., Prog. Photovolt: Res. Appl, 42 (8) (2019).
16. S. Buecheler et al., paper presented at the 7th International Workshop on CIGS Solar Cell Technology, Munich, Germany, (2016).

17. M. Yamaguchi et al., *J. Appl. Phys.*, 129, 240901 (2021).
18. N. Song, et al., *Appl. Surf. Sci.*, 459, 700-706 (2018).
19. F. I. S. E. Systems. ISE. Photovoltaics Report. <https://www.ise.fraunhofer.de/content/dam/ise/de/documents/publications/studies/Photovoltaics-Report.pdf>. (Last access September 1st, 2022).
20. M. Hadjab et al., *Int. J. Simul. Model.*, 42, 179–191 (2022).
21. P. Jackson et al., *Prog. Photovolt. Res. Appl.* 19, 894- 897 (2011).
22. I. Repins et al., paper presented at the 33rd IEEE Photovoltaic Specialists Conference San Diego, California, 11–16 (2008).
23. C. H. Huang, *J. Phys. Chem. Solids*, 69, 330–334 (2008).
24. K. Kim et al., *Solar Energy*, 155, 167–177 (2017).
25. S. Nacer and A. Aissat, *Appl. Phys. A*, 122:138 (2016).
26. B. Bibi et al., *J. Computat. Electron.*, 20, 1769–1778 (2021).
27. M. R. Mitroi et al., *Int. J. Photoenergy*, 7284367, 6 (2017).
28. P. Colter et al., *Crystals*, 8 (12) (2018).
29. M. Burgelman et al., *Thin solid films*, 361, 527-532 (2000).
30. A. Shalav, et al., *Appl. Phys. Lett.*, 86 (1), 013505 (2005).
31. A. Soheili et al., *Optik*, 222, 165461 (2020).
32. M. Benaicha et al., *J. Semicond.* 41, 032701 (2020).
33. A. Herguth, *Energy Procedia*, 124, 53–59 (2017).
34. K. Amri et al., *Energies*, 14, 3383 (2021).
35. O. Lundberg et al., *Thin Solid Films*, 480, 520–525 (2005).
36. S. Shirakata et al., *Sol. Energ. Mat. Sol. C.*, 93, 988–992 (2009).
37. M. Asaduzzaman et al., *Springer Plus*, 5, 578 (2016).
38. S.M. Sze and K.K. Ng, *Physics of semiconductor devices*, John wiley & Sons (2006).
39. S.R. Kodigala, Academic Press (2011).
40. C. W. Chen et al., *J. Mater. Chem. A*, 3 (29), 14985–14990 (2015).
41. J. Julayhi and T. Minemoto, *Physica Status Solidi C*, 10 (7), 1026–1030 (2013).
42. J. Li et al., paper presented at the 38th IEEE Photovoltaic Specialists Conference, Austin, TX, 1580–1583 (2012).
43. E. Klugmann-Radziemska, et al., *Sol. Energ. Mat. Sol. C.*, 94, 2275–2282, (2010).
44. M. Isah et al., *J. Alloy. Compd.*, 870, 15935 (2021).
45. F.M.T.Enam et al., *Optik*, 139, 397–406 (2017).
46. S. Sarker et al., *Solar Energy*, 225, 471–485 (2021).
47. H. Asif, et al., IEEE Region 10 Symposium (TENSYP), Dhaka, Bangladesh, 1221–1224 (2020).
48. A. Hoque et al., Proceedings of the International Conference on Mechanical Engineering and Renewable Energy (ICMERE) Chittagong, Bangladesh (2019).